Intrinsically bioactive cryogels based on platelet lysate nanocomposites for hemostasis applications

Bárbara B. Mendes[1,2], Manuel Gómez-Florit[1,2], Ana C. Araújo[1,2], Justina Prada[3], Pedro S. Babo[1,2], Rui M. A. Domingues[1,2], Rui L. Reis[1,2], Manuela E. Gomes[1,2*]*

[1] 3B's Research Group, I3Bs – Research Institute on Biomaterials, Biodegradables and Biomimetics, University of Minho, Headquarters of the European Institute of Excellence on Tissue Engineering and Regenerative Medicine, Avepark, Zona Industrial da Gandra, 4805-017 Barco – Guimarães, Portugal.

[2] ICVS/3B's – PT Government Associate Laboratory, Braga/Guimarães 4805-017, Portugal.

[3] UTAD, CECAV and Department of Veterinary Sciences, University of Trás-os-Montes and Alto Douro, 5001-801 Vila Real, Portugal.

Keywords: Platelet lysate, bioactive, cryogels, hemostatic

Abstract. The currently used hemostatic agents are highly effective in stopping hemorrhages but have a limited role in the modulation of the wound healing environment. Herein, we propose an intrinsically bioactive hemostatic cryogel based on platelet lysate (PL) and aldehyde-functionalized cellulose nanocrystals (a-CNC). PL have attracted great attention as an inexpensive milieu of therapeutically-relevant proteins, however its application as hemostatic agent exhibits serious constraints (e.g., structural integrity and short shelf-life). The incorporation of a-CNC showed to reinforce the low strength PL matrix by covalent cross-link its amine groups that exhibits an elastic interconnected porous network after full cryogelation. Upon blood immersion, the PL-CNC cryogels absorbed higher volumes of blood at a faster rate than commercial hemostatic porcine gelatin sponges. Simultaneously, the cryogels released biomolecules that increased stem cell proliferation, metabolic activity and migration as well as downregulated expression of markers of the fibrinolytic process. In a *in vivo* liver defect model, PL-CNC cryogels showed similar hemostatic performance in comparison with gelatin sponges and normal material-induced tissue response upon subcutaneous implantation. Overall, owing to its structure and bioactive composition, the proposed PL-CNC cryogels provide an alternative off-the-shelf hemostatic and antibacterial biomaterial with the potential to deliver therapeutically-relevant proteins in situ.

Introduction

Wound healing is a complex process orchestrated by the blood coagulation cascade and the cellular components of the immune system, which releases multiple cytokines, and induces crucial cellular and inflammatory pathways.[1, 2] Immediately after an injury occurs, it is of utmost importance to prevent excessive bleeding, as well as bacterial infection.[3] In healthy individuals, natural clotting process is relatively fast (within few minutes) and effective, even though severe bleeding accounts for approximately one third of total deaths in hospitals that occur due to traumatic injury events.[3-6] Thus, a prompt arrest of hemorrhage is essential for initial survival and for an optimal recovery in civilian and military trauma emergencies.[7, 8] Although the currently used polymeric and inorganic hemostatic formulations display good hemostatic capability, they still present several limitations.[9] For example, QuikClot® generates heat that might induce a thermal injury, whereas fibrin dressings have shown xenotoxicity due to the use of bovine origin products (e.g., thrombin).[10, 11] In addition, despite the versatility of the available hemostatic systems, the continued refinement of their composition should lead to formulations enabling not only effectively control hemorrhage and bacterial infection, but also promote tissue healing.

Platelets contain thousands of proteins that, with numerous post-translational modifications, results in over 1,500 identified protein-based bioactive factors, involved in coagulation, hemostasis, wound repair and regeneration.[12, 13] These factors include cytokines/chemokines (e.g., IL4, IL8), structural proteins (e.g., fibrinogen, fibronectin), and GFs (e.g., platelet-derived GF, vascular endothelial GF, transforming GF).[14, 15] Several hemostatic strategies have relied on the use of coagulation proteins, lyophilized platelets, platelet-derived nanovesicles or synthetic platelets have been reported.[16-18] Nevertheless, thrombotic complications, limited structural stability, variability, limited scalability or storage issues have been associated to these products.[19]

Among the different platelet-rich blood derivatives formulations, platelet lysate (PL) has a more reproducible preparation process and have shown comparatively lower batch-to-batch variability (when prepared from pools of samples/donors) than other blood derivatives formulations.[14, 20] The biological activity of PL has been leveraged to develop bioactive wound dressing to promote the healing process.[21, 22] However, sponge-like "dressings" showed limited structural integrity, which is necessary in hemostatic applications for a fast blood uptake, blood cells entrapment and stop bleeding.[21] Up to now, to the best of our knowledge, there are no previous reports on the use of PL on the development of hemostatic agents.

Different type of materials, such as injectable hydrogels[23, 24] or cryogels[25], are being proposed as hemostatic agents. In particular, cryogels can be defined as a class of hydrogels that introduced a new set of unique physical properties in the field of biomedical research.[26] Several of these systems have been use natural polymers (e.g., alginate and gelatin)[27, 28] as well as synthetic polymers (e.g., polyethylene glycol).[29] Their physical properties (e.g, interconnected macroporous structure and elasticity) play a key role on their large water absorption capability and fast shape recovery, which are crucial features for their application as hemostatic agents.[26] Recent attention has been paid to the use of nanomaterials as crosslinkers to effectively improve cryogels mechanical strength.[30, 31] For example, carbon nanotubes were used to reinforce chitosan cryogels and demonstrated the ability to quickly expand and mitigate bleeding *in vivo*.[25] However, concerns on the potential cytotoxicity of these nanoparticles has justified the search for better alternatives.[32] In this field, rod-shaped cellulose nanocrystals (CNC), known as the 'nature' carbon nanotubes, have been extensively applied in tissue engineering and regenerative medicine due to their mechanical strength, biocompatibility and high surface area.[31] Interestingly, 2,2,6,6-Tetramethylpiperidine-1-oxyl (TEMPO)-oxidized CNC/alginate composites dressings exhibited

structural, mechanical, and chemical stability while absorb a large abundance of wound exudate and improved blood cells adhesion.[33] More recently, nanocomposite based on oxidized bacterial nanocellulose have been shown to exhibit greater hemostatic capability and improved biocompatibility in comparison to unmodified oxidized bacterial nanocellulose or Surgicel gauze.[34] Nevertheless, although these biomaterials effectively control the hemorrhage (i.e., physical process), they do not possess intrinsically bioactive properties (i.e., biological process). It has been previously shown that aldehyde-modified CNC reinforced PL-based hydrogel network, fine-tuned hydrogel physical and biochemical microenvironment, and thus positively modulated the behavior of encapsulated stem cell.[35] Although these strategy demonstrated the outstanding biological properties of PL as an efficient engineered extracellular matrix (ECM) to promote regenerative wound healing outcomes, PL-CNC hydrogels approach do not exhibit a fast enough gelation nor the blood absorption capacity to be applied on the control of hemorrhages.[26]

In this study, we aim to mimic the *in vivo* wound healing process through the creation of an off-the-shelf intrinsically bioactive hemostatic PL-CNC cryogel. It is envisioned that the proposed hemostatic agent acts as a stable three-dimensional (3D) network to promote blood cells and blood-clotting factors entrapment while locally delivering the therapeutically-relevant PL-derived proteins. The physical and microstructural properties of isotropic and anisotropic PL-CNC cryogels are characterized. Then, the protein release from PL-CNC cryogels, as well as their antibacterial efficacy is evaluated. The impact of bioactive molecules released from PL-CNC cryogels on stem cell proliferation, migration and gene expression was assessed. Furthermore, the cryogels hemostatic potential was analyzed both *in vitro* and *in vivo* along with the evaluation of the tissue inflammatory response. We anticipate that this strategy will introduce a new approach

to manipulate the structural properties of blood-derived hemostatic materials, while potentiating the therapeutic effect of their biomolecules for promoting wound healing.

Experimental section

Precursors and cryogels production

Preparation of PL. Platelet concentrate collections, obtained from volunteer donation from healthy donors as by 2005/62/CE, were performed at *Serviço de Imuno-Hemoterapia – Centro Hospitalar de São João* (Portugal) provided under an approved institutional board protocol (ethical commission of CHSJ/FMUP approved at 18/13/2018). A pool of twelve platelet concentrate batches were subject to three freeze/ thaw cycles (−196 °C and 37 °C), and stored at −80 °C. Just before use, PL was thaw at room temperature (RT), centrifuged at 4000 x g for 5 minutes and filtered through a 0.45 μm pore filter to remove any cell debris or clots.

Preparation and characterization of aldehyde-modified CNC (a-CNC). CNC were extracted from microcrystalline cellulose powder (Sigma-Aldrich, USA) by sulfuric acid hydrolysis according to Bondeson et al. with minor modifications, as previously described.[35, 36] Then, vicinal hydroxyl groups on CNC's surface were converted to carbonyls by adding sodium periodate ($NaIO_4$) at a 1:1 molar ratio for 12 hours.[37] The chemical modification on a-CNC was confirmed by FTIR and CNC morphology was imaged by atomic force microscopy (AFM), as previously described.[35] The desired concentration of the working suspension was adjusted by concentrating it against poly(ethylene glycol) (average MW 20,000 kDa, Sigma-Aldrich, USA) using benzoylated cellulose dialysis membranes (2000 Da NMWCO, Sigma-Aldrich, USA).

PL-CNC cryogels production. PL-CNC cryogels were prepared blending PL with a-CNC at 1:1 volume ratio. A double-barrel syringe L-system (1:1 from Medmix, Switzerland) with a static mixer tip (Medmix, Switzerland) was used to homogenously extrude the cryogels precursor solutions into square molds or into syringes with the tip cut to make it blunt (1 mL SOFT-JECT®, inner diameter of 4.7 mm). Barrel 1 was filled with PL and barrel 2 with a-CNC aqueous dispersions (1.2 to 2.4 wt.%). After casting into the molds or syringes, the cryogel precursors were frozen at -80ºC and subsequently freeze-dried until full cryogelation. Anisotropic structured cryogels were also prepared (described in supplementary information). Cryogels formulations were named according to their final a-CNC concentrations: 0 wt.% (PL-CNC 0), 0.6 wt.% (PL-CNC 0.6) and 1.2 wt.% (PL-CNC 1.2).

Physical characterization of cryogels

Microstructure. PL-CNC cryogels were freeze-fractured in liquid nitrogen to expose their inner structures, and then sputter coated (30 seconds at 20 mA, Cressington) with gold prior observation in a scanning electron microscopy (SEM, JSM-6010LV, JEOL, Japan). Isotropic and anisotropic PL-CNC formulations (7 x 7 x 5 mm, n=5) were also scanned using X-ray scan micrograph (micro-CT; SkyScan 1272; Bruecker, Kontich, Belgium), at a resolution of 10 µm, reconstructed using the software NRecon (Version: 1.6.6.0, Skyscan), and analyzed on CT analyzer (Version: 1.17.0.0, Skyscan) (for more information please see supplementary information).

Mechanical characterization. Universal Mechanical Testing Machine (Instron 5540) equipped with a load cell of 1 kN was used to conduct unidirectional compression tests. The hydrated (2 hours in PBS) anisotropic and isotropic PL-CNC specimens (7 x 7 x 5 mm, n=5) were set on the

lower plate and compressed by moving the upper plate at a compression rate of 1 mm per minute at RT. For cyclic tests, isotropic PL-CNC 1.2 formulation was subjected to three successive loading and unloading cycles at a compression rate of 1 mm per minute and ε = 50%. The obtained stress-strain curves were used to calculate the Young's modulus (i.e. the average slope of the stress-strain curve in the initial linear region) in order to study cryogels structural integrity and their capacity for recovery.

Weight loss. Isotropic and anisotropic PL-CNC cryogels were incubated in 1.5 mL of phosphate buffered saline (PBS) pH=7.4 at 37 °C for 2 hours. After removing the excess of PBS, the initial mass of the cryogel was measured (M_i) and successively weighed at different time points (M_f) to determine the weight loss (%), according to Equation 1. The results are expressed as an average of five samples.

$$\text{Weight loss} = \frac{Mi - Mf}{Mi} \times 100 \qquad \text{(Equation 1)}$$

Protein release from cryogels

Delivery of PL-CNC cryogels releasate.*:* PL-CNC cryogels (V= 0.3 mL) were incubated in 1 mL of α-MEM with 1% antibiotic/antimycotic solution (i.e., without serum supplementation) at 37 ºC. At different time points (5 minutes, 6 hours, 1, 3, 5 and 7 days of incubation), the supernatant was collected and replaced with fresh cell culture medium. The timepoints were named as follows: D0 (5 minutes), 6H (6 hours), D1 (1 day), D3 (3 days), D5 (5 day) and D7 (7 days). After 1 week, PL-CNC cryogels were digested in 200 U. mL^{-1} *Trichoderma sp.* Cellulase (Sigma-Aldrich, USA,3-10 U. mg^{-1} solid). Total protein content in the diluted supernatant of PL-CNC formulations (n=3) was quantified according to the manufacturer's instructions using Coomassie (Bradford)

protein assay kit (Thermo Scientific, USA). Platelet-derived growth factor-BB (PDGF-BB) and vascular endothelial growth factor (VEGF) content in the releasates of PL-CNC cryogels at D0 timepoint (n = 3) were quantified using a human PDGF-BB and VEGF DuoSet enzyme-linked immunosorbent assay (ELISA) kit (R&D systems, biotechne, USA), according to the manufacturer's instructions.

Antibacterial activity

Escherichia coli and *Staphylococcus aureus* reduction analysis: The antibacterial activity of the cryogels was tested against *Escherichia coli* (*E. coli*; ATCC 25922 Gram negative bacteria) and *Staphylococcus aureus* (*S. aureus; ATCC 25923*, Gram positive bacteria), as previously described.[38] Bacterial cultures were grown in Tryptic Soy Broth medium at 37 °C overnight with agitation (150 rpm). Bacterial cells were centrifuged at 9000 x g for 5 minutes at 4 °C and washed twice with sterile PBS. Then, 10 µL of 1-2 x 10^6 CFU. mL^{-1} bacterial suspension in PBS was added onto PL-CNC cryogels surface and incubated for 2 hours at 37 °C. Afterwards, 1 mL of PBS was added to each well and 10 µL of the suspension was plated on the Tryptic Soy Agar plates. CFUs were counted after 24 h of incubation at 37 ºC. 10 µL of bacterial suspension in PBS (1-2 x10^6 CFU. mL^{-1}) was used as a negative control. Tests were repeated three times for each group and the results were expressed as bacterial reduction (%), see Equation 2.

$$\text{Bacterial reduction} = \frac{\text{colonies count of control} - \text{survivor count on sample}}{\textit{colonies count of control}} \text{ x } 100 \qquad \text{(Equation 2)}$$

Hemostatic properties

Whole blood collection. Human blood samples were drawn from healthy donors at *Serviço de Imuno-Hemoterapia – Centro Hospitalar de São João* (Portugal) provided under an approved

institutional board protocol (ethical commission of CHSJ/FMUP approved at 18/13/2018). It was collected in sterile BD Vacutainer® tubes (BD-Plymouth, UK), which contains 0.129 M sodium citrate at 9:1 ratio. The collected whole blood was stored at RT.

Blood absorption rate. PL-CNC cryogels and commercial hemostatic porcine gelatin sponges (Gelita-Spon® Standard, Gelita® Medical, Germany) were weighed (M_d), and incubated with whole blood for 5, 30, 60 and 180 seconds. The samples were immediately transferred to the clean gauze for 10 s to remove the unabsorbed blood and weighed (M_w). The adsorption rate (%) was calculated using Equation 3. Images of the samples after 180 seconds of incubation in whole blood were taken.

$$\text{Blood absorption rate} = \frac{\text{Mw}-\text{Md}}{\text{Md}} \text{ x } 100 \quad \text{(Equation 3)}$$

Hemolytic activity assay. Whole blood was centrifuged at 116 x g for 10 minutes, washed three times with PBS, and then the obtained erythrocytes were diluted to a final concentration of 5 vol.% as previously reported.[25, 39] Afterwards, 10 mg of each sample was added to 500 µL of erythrocyte suspension. PBS buffer (0% lysis) and 0.1 vol.% Triton X-100 (100% lysis) were also added to the erythrocyte suspension, and served as the negative and positive control, respectively. After incubation for 1 hour at 37 °C in a shaking incubator chamber, the mixture was centrifuged at 120 x g for 10 minutes. 100 µL of the obtained supernatants were transferred into a 96-well clear plate, and the absorbance was measured at 540 nm to determine the hemolytic ratio (%), see Equation 4.

$$\text{Hemolytic ratio} = \frac{\text{Test sample}-\text{Negative control}}{\text{Positive control}-\text{Negative control}} \text{ x } 100 \quad \text{(Equation 4)}$$

Blood cells adhesion. Whole blood was added dropwise into PL-CNC cryogels and commercial absorbable gelatin sponge hemostat (7 x 7 x 3 mm), and then incubated for 5 minutes at 37 °C as described in the literature.[25, 33] In platelet adhesion studies, whole blood was centrifuged at 300 x g for 10 minutes and then the upper phase (i.e., platelet-rich plasma) was added dropwise to the sample and incubated for 1 hour at 37 °C. All samples were washed three times with PBS to remove the non-adherent and loosely attached cells, and then fixed with 2.5 vol.% glutaraldehyde (Merck, Germany) for 2 hours. After fixation, samples were solvent exchanged from water to ethanol (ethanol gradient 25, 50, 75 and 99.9 vol.%) for 4 hours, and then dried overnight at RT. Finally, the samples were sputter coated (30 seconds at 20 mA, Cressington) with gold prior observation in a SEM.

Cellular experiments

Cell isolation and expansion. Human adipose-derived stem cells (hASCs) were obtained from lipoaspirate samples of the abdominal region of healthy donors undergoing plastic surgery under the scope of an established protocol with Hospital da Prelada (Porto, Portugal), and with the approval of the Hospital Ethics Committee. The hASCs isolation were performed using a previously optimized protocol.[40] hASCs were maintained in α-MEM supplemented with 10% fetal bovine serum (FBS) and 1% antibiotic/antimycotic solution at 37 ºC, 5% CO_2.

Cell viability. $5x10^5$ hASCs were seeded on the cryogels surface. After 90 minutes, α-MEM with 1% antibiotic/antimycotic solution (i.e., without FBS supplementation) was added to the cryogel formulations and changed every two days. On days 3 and 7, cellular viability was assessed using 1:500 vol.% Calcein AM (Thermo Fisher Scientific, USA) and 1:1000 vol.% propidium

iodide (Thermo Fisher Scientific, USA) staining for 15 minutes at 37 °C. PL-CNC cryogels formulations were washed twice with PBS and visualized using confocal microscope TCS SP8 (Leica Microsystems, Germany).

Cell proliferation. 1.66 x 10^4 hASCs per 1 cm^2 were seeded in 48-well plates for 24 hours in α-MEM supplemented with 10% FBS and 1% antibiotic/antimycotic solution. The medium was removed and replaced with 200 µL of PL-CNC cryogel and gelatin sponge releasates collected after D0, 6H, D1, D3, D5 and D7. After 24 hours, the metabolic activity and proliferation of hASCs were evaluated using Alamar Blue assay kit (Bio-Rad, USA) and Quant-iT PicoGreen dsDNA assay kit (Thermo Fisher Scientific, USA), respectively. Briefly, hASCs were incubated with alamar blue solution for 4 hours at 37 °C. The alamar blue fluorescence was assayed at 535 (excitation) and 600 (emission) nm. After washing twice with PBS, ultrapure water was added to the cell culture plate and frozen at -80 ºC. The released DNA was quantified following manufacturer's instructions (Thermo Fisher Scientific, USA). Metabolic activity results (i.e. alamar blue fluorescence) were normalized with its respective cell number (i.e. DNA content) to quantify metabolic activity per cell.

Scratch assay. hASCs at a density of 7.7×10^4 per 1 cm^2 were seeded on 96-well plates, as previously described.[41] After 24 hours, a confluent cell monolayer was formed, and the monolayer was scraped with a 0.1–10 µL sterile pipette tip (0.57 mm) in a straight line to create a scratch. The medium was removed, the wells were washed with PBS, and replaced with 100 µL of PL-CNC cryogel and gelatin sponge releasates collected at D0. Cell migration was imaged and monitored using an inverted phase-contrast microscope for 48 hours. The images were

quantitatively analyzed using Tscratch software to calculate open wound area (%), see Equation 5.

$$\text{Open wound area} = \frac{\text{100 x open wound area at 48 hours}}{\text{open wound area at 0 hours}} \quad \text{(Equation 5)}$$

Gene expression analysis. After scratch assay analysis, the releasates were removed, and hASCs were washed with PBS. Then, total ribonucleic acid (RNA) was isolated using TriReagent® (Sigma-Aldrich, USA), according to the manufacturer's protocol. Total RNA was quantified at 260 nm using a NanoDrop spectrophotometer (Thermo Fisher Scientific, USA). The same amount of RNA (225 ng) was reverse transcribed to complementary DNA according to the protocol of the supplier (qScript cDNA Synthesis Kit, Quanta Biosciences, USA). Aliquots of each cDNA sample were frozen until the PCR reactions were carried out. Real-time PCR was performed for two reference genes, glyceraldehyde-3-phosphate dehydrogenase (GAPDH) and β-actin and target genes (Table S1), as previously described.[35] All samples were normalized by the geometric mean of the expression levels of β-actin and GAPDH as explained in [42]. Finally, fold changes were expressed relative to the expression in the gelatin sponge control group.

In vivo assay

Housing and maintenance of animals. All animal procedures were based upon the ''3Rs" policy (Replacement, Reduction and Refinement) and were carried out after approval by the Ethics Committee of University of Minho and Portuguese Licensing Authority (DGAV). Total of 16 Sprague-Dawley male rat of 7 weeks old and average weight of 185–210 g (Envigo, UK) were used in this study. Each rat was anesthetized by intraperitoneal injection: Domitor INJ 1 mg. mL^{-}

[1] (Medetomidine 1 mg. kg^{-1}, Novavet, Braga, Portugal) and Imalgene 1000 INJ 100 mg. mL^{-1} (Ketamine 75 mg. kg^{-1}, Novavet, Braga, Portugal).

Hemostatic test on a standardized rat liver trauma model. The liver of the rat was exposed by abdominal incision. A pre-weighed filter paper on a paraffin film was placed beneath the liver and the liver bleeding was induced using an 18 G needle. Immediately after the injury, PL-CNC 0.6 and 1.2 cryogels, and a commercial absorbable gelatin sponge (n=6) were applied on the site of lesion until bleeding stopped. The weight of the filter paper with absorbed blood (blood loss) was measured, as well as the time to restore hemostasis (hemostasis time). The rats were euthanized by intracardiac injection of excess Eutasil 200 mg. mL^{-1} (pentobarbital sodium, Novavet, Braga, Portugal). Samples were fixed with 2.5 % glutaraldehyde (Merck, Germany) for 2 hours. After fixation, samples were solvent exchanged from water to ethanol (ethanol gradient 25, 50, 75 and 99.9 vol.%) for 4 hours and then dried overnight at RT. Finally, the samples were sputter coated (30 seconds at 20 mA, Cressington) with gold prior observation in a SEM.

Host response evaluation. The rat hair was shaved at the implantation area, followed by disinfection with 70% ethanol and iodine. In each rat, four skin incisions (1 cm length) were made in the dorsal midline, two close to the head (CH) and the other two far from the head (FH). PL-CNC 0.6 and 1.2 formulations, saline solution, and a commercial absorbable gelatin sponge were implanted into the respective pockets, followed by skin suturing. The rats were euthanized 7 and 14 days postsurgery by intracardiac injection of excess Eutasil 200 mg. mL^{-1} (pentobarbital sodium, Novavet, Braga, Portugal). The implanted materials were retrieved along with the surrounding tissue to histological analysis. In the pockets where we did not observe any lesion in

the tissues, we collected samples of the normal skin and subcutaneous tissue. The explants were fixed with 10 vol.% formalin and transferred to histological cassettes for paraffin-embedding. Samples were then serially sectioned using a microtome and stained with hematoxylin & eosin (H&E) to further microscopic examination.

Local biological effects assessment after samples implantation. The evaluation of fibrosis, necrosis and angiogenesis was performed according to ISO 10993-6, 2007 biological evaluation of medical devices. The results were expressed in ordinal scale units.

Statistical analysis

The statistical analysis of data was performed using GraphPad PRISM v 7.0. Shapiro-Wilk normality test and one-way analysis of variance (ANOVA) was used to analyze experimental data, followed by the Tukey post hoc or Krustal-Wallis test for multiple comparisons. Results are presented as mean ± standard deviation.

Results and Discussion

An ideal hemostatic agent should allow a high blood uptake capacity, a rapid blood triggered shape recovery and absorption speed, inherent antibacterial ability, robust mechanical strength, as well as, it should be biocompatible, ready and easy to use, lightweight, stable, and inexpensive.[7] In order to explore the full potential of PL-based cryogels for hemostatic applications, it is fundamental to improve their structural integrity and to extend their shelf life while preserving the therapeutic potential of PL-derived biomolecules such as cytokines, antimicrobial peptides, soluble adhesion molecules and coagulation factors.[43] It is known that cryogels production

methods have impact on the material porous structure and lamella densification, and these properties directly affect their blood adsorption capability.[44] Thus, to evaluate the impact of different microstructures on the functional material performance, cryogels with isotropic or anisotropic pore organization were produced by applying uniform or unidirectional temperature gradient during the cryogelation process, respectively.

Preparation and physical characterization of PL nanocomposite cryogels

During gelation at subzero temperatures, the aqueous component freezes and forms ice crystals that act as pore-forming agents, excluding solute (i.e., PL proteins and a-CNC) from the ice lattice into the space between the growing ice crystals.[45] The application of non-directional or unidirectional temperature gradients, has been used to determine the anisotropy degree of the resulting porous structure upon freeze-drying.[46] Herein, PL and a-CNC were homogeneously extruded into a square mold in equal parts and submitted to non-directional and unidirectional freeze-casting at −80 °C, and then PL-CNC formulations were freeze-dried, obtaining isotropic and anisotropic PL-CNC cryogels respectively. First, to assess the stability of PL-CNC 0, 0.6 and 1.2 wt.% cryogels, the formulations were immersed in PBS and the changes in the shape of cryogels were recorded (Fig. 1a and Fig. S1a). The cryogel solely based on PL showed a fast solubilization, losing the preformed 3D structure (Fig. 1a), whereas PL-CNC formulations composed of 0.6 and 1.2 wt.% CNC content maintained their structure and showed a high mold fidelity (Fig. 1a and S1a). These findings suggest that two different factors are pivotal to provide cryogels structural integrity and to prevent their disintegration upon cryogel hydration; (1) the chemical covalent cross-linking between a-CNC and the amine groups of PL proteins through reversible Schiff base bonds.[35, 47]; and (2)the densification of a-CNC nanomaterials and PL-

proteins (i.e., polymers) in the pore walls during ice crystals growth.[48] , are pivotal factors to provide cryogels structural integrity and to prevent their disintegration.

PL-CNC cryogels structure was evaluated by micro-computed tomography (μ-CT) and SEM (Fig. 1 and Fig. S1). In line with previous cryogelation studies, isotropic PL-CNC cryogels revealed a disordered pore structure (Fig. 1b), with a mean pore diameter around 110 μm (table S2), whereas anisotropic PL-CNC cryogels exhibited aligned pores along the freezing direction (Fig. S1b and S1c-i and ii). In addition, isotropic PL-CNC cryogels showed markedly larger pore diameter (around 110 μm) and a higher pore interconnectivity (around 95%) in comparison with anisotropic PL-CNC cryogels (Table S2 and S3). Interestingly, isotropic PL-CNC 0.6 and 1.2 cryogels exhibit similar porosity (87.6 ± 3 vs. 88.9 ± 1.5 vol.%), pore diameter (112.3 ± 51.3 vs. 105.6 ± 13.2 μm) and interconnectivity (96.88 ± 2.5 vs. 96.9 ± 2.5). These results indicate that fabrication conditions (e.g., freezing process) are the driving force for the observed structural differences, which are not changed by varying CNC concentration (0.6 vs. 1.2 wt.%).

Since blood absorption capacity is crucial to accelerate blood cells entrapment to form a blood clot, the water uptake was evaluated in isotropic and anisotropic cryogels.[25, 28] Regarding the ability to adsorb liquids, isotropic PL-CNC cryogels exhibited a faster water uptake capability (Fig. S1f). Most likely, it is a direct consequence of the above reported larger pore size and highly interconnected structure of the isotropic formulations. Therefore, isotropic PL-CNC cryogels were selected for further physical and biological characterization to be applied as a potential hemostatic agent.

Cryogels often lack mechanical strength mainly due to their macroporous morphology, which is formed during the cryogelation process.[48, 49] CNC have been used as biocompatible reinforcement nanofillers in low strength matrices due to its high stiffness (200-220 GPa) and axial elastic

modulus (110 to 220 GPa).[30, 31] To confirm the benefits of CNC incorporation, the mechanical properties of PL-CNC cryogels were evaluated on swollen conditions (Fig. 1c to e, Fig. S1d). While it was impossible to determine Young's modulus of PL-CNC 0 due to its fast solubilization (Fig. 1a), PL-CNC 1.2 modulus (4.4 ± 1.1 kPa) was almost the double of the modulus of PL-CNC 0.6 (2.3 ± 0.3 kPa). As expected, at higher concentration of a-CNC, there is an increase of total cryogel crosslinking density, which results in stiffer cryogels.[47]

Intense efforts have been made to design hemostatic agents that are able to control irregularly shaped, deep and noncompressible wounds while applied in a minimally invasive strategy.[50] Therefore, a hemostatic agent that once applied to the wound, absorb blood, rapidly expand and gently provides an outward pressure within the wound cavity is still highly needed. Accordingly the obtained mechanical properties results, the shape memory capacity of isotropic PL-CNC 1.2 formulation was evaluated (Fig. 1d-i and e, and Movie 1). PL-CNC 1.2 cryogels could be compressed up to 50% strain level without being mechanically or structurally damaged. Upon load removal, the elastically deformed cryogels recovered their original shape as the surrounding water was reabsorbed, exhibiting a fast deformation reversion (~on the order of seconds), Fig. 1e. Then, PL-CNC 1.2 cryogels were subjected to three successive compression cycles with a deformation speed of 1 mm per minute (Fig. 1d-i). Even though the cryogel exhibited hysteresis loops comprising the loading and unloading phases that indicates energy dissipation, there is an overlap of the cyclic stress-strain curves with comparable and reproducible compressive strength values. These results confirmed that PL-CNC cryogels possess a good mechanical strength and high compression resilience under continuous and dynamic compression as well as withstand extensive deformations without being destroyed. These findings are in agreement with previous results where the incorporation of high aspect ratio and high stiffness nanoparticles such as carbon

nanotubes in cryogels composition led to nanocomposite materials displaying similar unique mechanical characteristics.[25, 26] Remarkably, after 6-month of storage at RT, cryogels high elastic behavior was still evident, demonstrating its structural resilience to long-term storage (Fig. 1d-ii). When PL-CNC cryogels were extruded from a syringe, they also showed an immediately water absorption capability while maintaining its strength and easy handling (Movie 2 and 3). These findings demonstrate the versatile applications of PL-CNC cryogels. They exhibit a fast shape recovery capacity, property of interest to rapidly cease deep and noncompressible wounds, as well as a high structural integrity that allows a simple handling and its easy removal from the wound bed (if required).

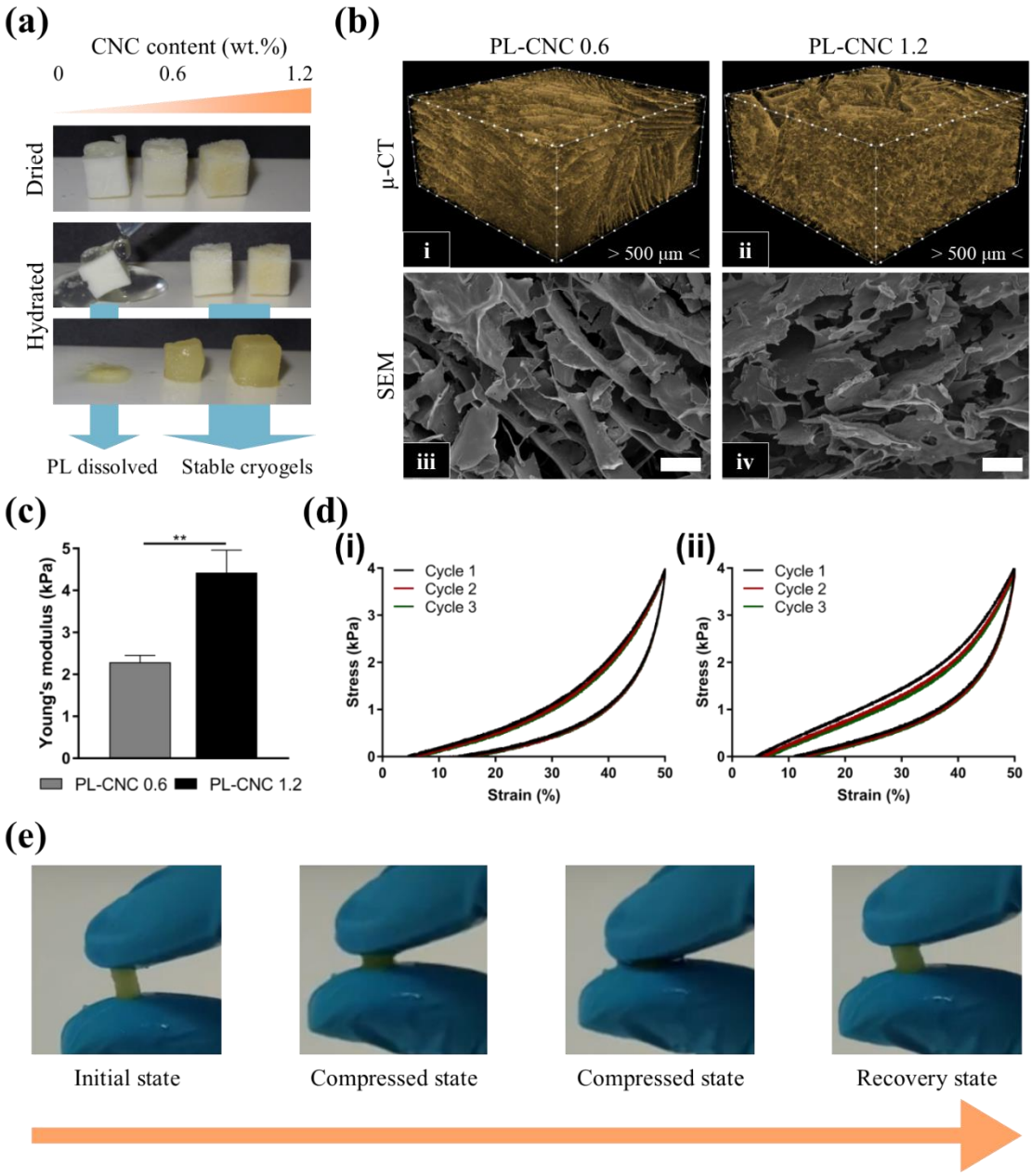

Figure 1. Physical properties of the cryogels formulations. (a) Cryogels stability after immersion in PBS. (b) Microstructure evaluation by SEM (i-ii) and μ-CT (iii-iv). (c) Young's modulus from the uniaxial compression stress–strain curves. (d) Three successive loading and unloading cycles of PL-CNC 1.2 at ε = 50% in fresh (i) and 6 months stored samples (ii). (e) Photographs

representing the shape memory property and rapid recovery speed of PL-CNC 1.2 cryogels after absorbing water. Statistical significance: **, $P < 0.01$. Scale bar: 50 μm (b-iii and iv).

Protein release from PL-CNC cryogels

Wound healing is a complex process that involves the interplay of multiple cell populations and soluble mediators in a highly organized and orchestrated manner.[1, 2] Generally, upon injury, platelets in wound site suffer degranulation through the activation by any thrombogenic agent, which induce morphological changes and the release of bioactive factors from their α- and dense granules, and lysosomes into the local wound environment.[51] These factors include clotting agents (e.g., thrombin, von Willebrand factor), cytokines/chemokines (e.g., IL4, IL8), structural proteins (e.g., fibrinogen, fibronectin), microbicidal proteins (e.g., β-lysin, complement proteins), ions (e.g., calcium), membrane proteins (e.g., CD63) and GFs (e.g., platelet-derived GF, vascular endothelial GF, transforming GF) mediate several wound healing stages.[14, 15] Besides the recruitment of immune cells and the initiation of the clot formation during hemostasis, platelet-derived biomolecules have also been shown to be crucial mediators in several further wound healing stages, for example immunomodulatory processes, antibacterial activity, inflammatory response, and tissue repair and regeneration.[14] In a biomimetic approach, platelet concentrate units were mechanically disrupted to promote the release of these biomolecules milieu in a reproducible large scale and cost-effective manufacturing. Upon full cryogelation, a-CNC act as crosslinkers of PL proteins to produce a scaffold that close resembles fibrin network physical support.

Once PL-CNC cryogels are applied in the wound site, it is crucial the adequate maintenance of its mechanical strength and porosity, blood cells infiltration and local delivery of PL-derived proteins at the bleeding site.[7, 52] Thus, the structural integrity of PL-CNC cryogels over 7 days was

evaluated by measuring the weight loss and total protein content release assays, Fig. 2a. First, weight losses were monitored as a measure of cryogels degradation (Fig. 2a-i). Both formulations undergo weight decrease over the time, though PL-CNC 0.6 showed a markedly higher weight loss (45.1 ± 6.2 %) in comparison with PL-CNC 1.2 (19.4 ± 2.7 %). As previously anticipated, the formulation with high precursor content (1.2 wt.%) led to an increase of crosslinking degree between the a-CNC and amine groups of PL-derived proteins (i.e., chemical crosslinking) as well as to a more tightly packed structure that increased nanomaterial/protein interactions (i.e., physical crosslinking), which is sufficient to maintain its initial structural integrity.

The release of the protein cryogels content was quantified to evaluate the potential of cryogels as biomolecules delivery systems (Fig. 2a-ii). Upon incubation for 5 minutes (D0), both conditions exhibited an initial burst release, followed by an apparent "plateau" profile. This protein release profile can be explained by the simple diffusion of the proteins non-bound to the cryogel at the first minutes, as previously demonstrated in other PL crosslinked scaffolds.[53, 54] At the end of the experiment, PL-CNC 0.6 cryogel released 73.9 ± 11.3 wt. % of total protein content whereas PL-CNC 1.2 delivered 85.4 ± 5.9 wt. % of total protein content. Considering the low amount of CNC used and the open macroporous cryogel structure, this initial burst release of biomolecules into the solution was expectable. Then, it was quantified the release of PL-derived chemotactic and proangiogenic GFs, namely platelet-derived GF and vascular endothelial GF, respectively (Figure 2b). The immunodetection of both GFs demonstrates that their bioactivity is preserved during the cryogelation process. These GFs are known to plays a pivotal role on boosting the cells mitogenic activity and to favor endothelial sprouting, which are crucial to promote wound healing *in vivo*.[55, 56] Together, these results contribute to further demonstrate the bioactivity of the proposed PL-CNC cryogel system.

It is worth to mention that the weight assay was conducted after 2 hours of incubation in PBS, thus considering the burst proteins release and the remained water, it is expected a difference on cryogels weight and protein release assays. Accordingly, this material should not be infused into an aqueous solution prior to use, since it exhibited an initial burst release of the bioactive molecules, envisioning improved functionalities when applied dry.

Antibacterial properties

Conferring antibacterial properties to hemostatic sponges might bring several benefits since the continued presence of a high bacterial load in wounds increases inflammation and delays the healing process.[2] Interestingly, platelets have a significant and direct role in the antimicrobial host defense, mainly due to the release of a wide variety of host defense peptides (including antimicrobial peptides) in response to injury, namely platelet factor-4, RANTES, connective tissue activating peptide 3, platelet basic protein, thymosin β-4, fibrinopeptide B, fibrinopeptide A and thrombocidins, which are able to kill bacteria by cytoplasmatic membrane permeation and cell lysis.[57-59] Moreover, our group has previously demonstrated that genipin-crosslinked PL patches exhibited an antibacterial effect by preventing the adhesion, proliferation and biofilm formation by S. aureus, which can be related to PL proteins presence.[60] Therefore, the antibacterial activity of the cryogels developed in this study was assessed against Gram positive S. aureus and Gram negative E. coli bacteria (Fig. 2b). Remarkably, PL-CNC cryogels showed significant reduction of S. aureus and E. coli survival. The reduction of S. aureus survival in the presence of PL-CNC was 73.1 ± 16.4 % (PL-CNC 0.6) and 96.3 ± 1.3 % (PL-CNC 1.2), Fig. 2b-i and iii. Moreover, the inhibitory effect of PL-CNC cryogels against E. coli bacteria was found to be similar between PL-CNC 0.6 (91.4 ± 7.9 %) and PL-CNC 1.2 (91.2 ± 8.2 %) groups, Fig. 2b-ii and iv. Recently, we

have shown that upon contact with PL, a “hard” corona is formed on CNC’s surface, which contains, among other proteins, different host defense peptides.[61] The solid-phase presentation of protein and peptide signaling molecules is recognized to increase the half-life and boost the bioactivity of these liable molecules.[62] Based on these concepts, we hypothesize that the sequestration/retention and solid-phase presentation of these peptides might contribute to observed antibacterial activity upon contact with S. aureus, which is higher in cryogels with higher CNC content. Thus, PL-CNC cryogels might be used as prophylactic agents to impede bacterial infection, although further investigation is needed to fully understand how to modulate the observed antibacterial activity.

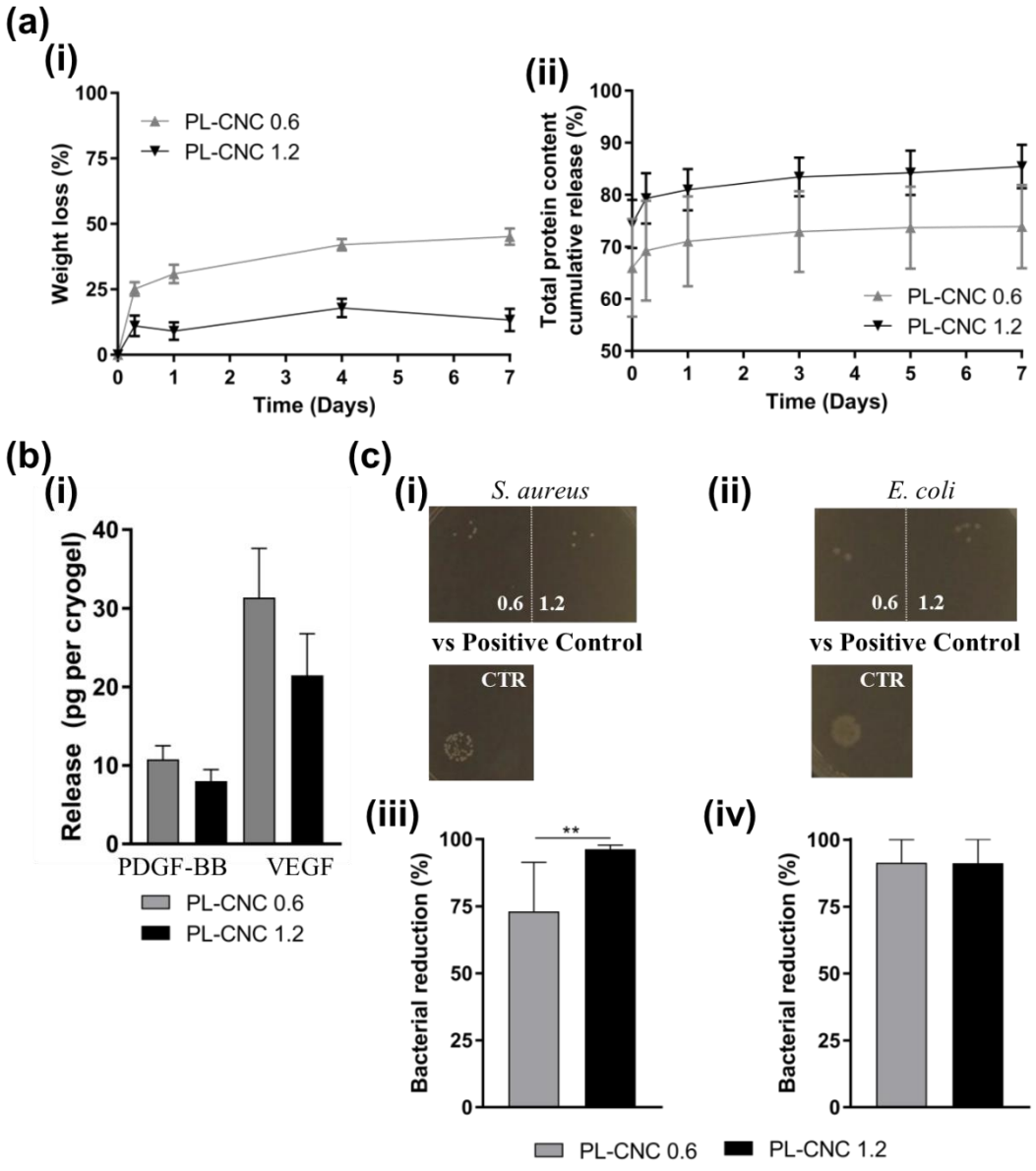

Figure 2. Release of bioactive molecules from PL-CNC cryogels. (a) Weigh loss (i) and release kinetics of bioactive proteins from PL-CNC cryogels over 7 days (ii). (b) Release of VEGF and PDGF-BB in cell culture medium at D0 (5 minutes). (c) Antibacterial activity of the PL-CNC 0.6 (0.6), PL-CNC 1.2 (1.2) and 10 µL of bacterial suspension in PBS (CTR) against S. aureus (i-iii) and E. coli (ii-iv), photographs of agar plates (i and ii) and bacterial reduction quantification (iii and iv). Statistical significance: **, $P < 0.01$.

In vitro hemostatic potential

In order to manage an uncontrolled post-traumatic hemorrhage, it is critical a rapid blood absorption to accumulate blood cells and to activate coagulation factors, which, ultimately, will effectively control an *in vivo* hemorrhage.[7] Hence, the hemostatic properties of PL-CNC cryogels *in vitro* were studied and compared with a commercial hemostatic porcine gelatin sponge (Gelita-Spon® Standard, Gelita® Medical, Germany).

As a first screening for hemostatic potential, both PL-CNC cryogel and gelatin sponge control formulations were immersed in whole blood. PL-CNC cryogels revealed a homogeneous absorption and maintenance of initial shape integrity (Fig. 3a). On the other hand, commercial gelatin sponges of the same size (7 x 7 x 3 mm) exhibited a structural collapse without the recovery of its original shape that was exacerbated when gelatin samples were handled. As previously observed in water absorption test, it seems that the interconnectivity of PL-CNC cryogels is adequate to promote blood cells infiltration. During the first 5 seconds, gelatin sponges showed the lowest absorption potential, reaching a maximum of 354.5 ± 77.1 %, which was significantly lower than the cryogels absorption capacity. PL-CNC 0.6 cryogels showed a faster blood absorption than PL-CNC 1.2 cryogels, and after 30 seconds they reached a blood absorption plateau at 1158.2 ± 156.7 wt. % and 1260.6 ± 40.8 wt. % of their initial dry weight, respectively (Fig. 3b). It is worth mentioning the importance of the large surface area, macroporous morphology and high pore interconnectivity in the obtained swelling capacity of the control and test samples, which are undoubtedly much higher than those of traditional hydrogels.[26] Moreover, PL-CNC groups exhibited higher blood absorption capacity than other hemostatic agents, for example mesoporous chitosan sponge.[39] Remarkably, the macrostructural integrity of PL-CNC cryogels is decisive to obtain a higher blood uptake than the water-soluble gelatin sponge.

Once hemostatic agents are applied at the bleeding site, blood is the first component to interact with them. The material-to-blood direct contact can promote the loss of red blood cells (RBC) membrane integrity (hemolysis) leading to the leakage of hemoglobin into blood plasma, which can trigger specific pathophysiologies.[63] Thus, the hemocompatibility of materials was evaluated by *in vitro* hemolysis ratio (Fig. 3c) as well as RBC (Fig. 3d) and platelets (Fig 3e) adhesion and morphology on the different cryogel formulations. Upon incubation with a RBC suspension, hemolysis ratios of PL-CNC cryogels, gelatin sponge, PBS (positive control) and Triton X-100 (negative control) were determined (Fig. 3c). PL-CNC cryogels and gelatin sponge supernatants exhibited a light yellow color similar to PBS, whereas Triton-X was bright red due to the release of hemoglobin into the liquid (Fig. 3c-i). For the quantitative hemolysis ratio, gelatin sponge showed the lowest value of 1.9 ± 0.5 %, but not statistically significant to PL-CNC 0.6 (3.7 ± 2.0 %) and PL-CNC 1.2 (2.5 ± 0.6 %) groups (Fig. 3c-ii), indicating that these are non-harmful for RBC. The obtained hemolysis ratios values are comparable with previously reported hemostatic materials, thus confirming cryogels hemocompatibility.[25]

The three groups showed a large number of blood cells (i.e. RBC and platelets) adhering to their surfaces (Fig. 3d and e). High-magnification SEM images of blood cells clearly display two type of cells: (1) round cells with an indented center and biconcave disc shape (normal RBC) that tend to form aggregates ("rouleaux") [64] and (2) spherical cells covered with abundant fine uniform crenations (echinocytes or altered RBC), Fig. 3d-iii, vi and ix. The presence of echinocytes can be explained by the exposure to anticoagulants or staining techniques, but RBC are able to recover their discoid shape when re-introduced into fresh plasma.[65] Concerning platelet adhesion on hemostats surface, PL-CNC cryogels and gelatin sponge were incubated for 1 hour with PRP (Fig. 3e). Platelets of 2-3 µm diameter adhered to the material's surface and exhibit a flattened

morphology with projections of pseudopodia and lamellipodia, which is an indicator of platelet activation.[25, 33, 66] The adhesive interactions mediated platelet to platelet aggregation that produced a tenaciously adherent mass of platelets, being more evident on PL-CNC 0.6 cryogel formulation (Fig. 3e-ii). We hypothesize that the observed fast blood absorption of PL-CNC 0.6 cryogel promoted an initial higher adhesion of platelets and produced a more evident platelet aggregate in comparison with the other two tested formulations. Altogether, the results indicate that PL-CNC cryogels have a higher uptake of blood than the control, which enhances blood cells adhesion, platelets activation and aggregation, and possible release of coagulation factors that will clearly contribute to their *in vivo* blood-clotting capability.[43]

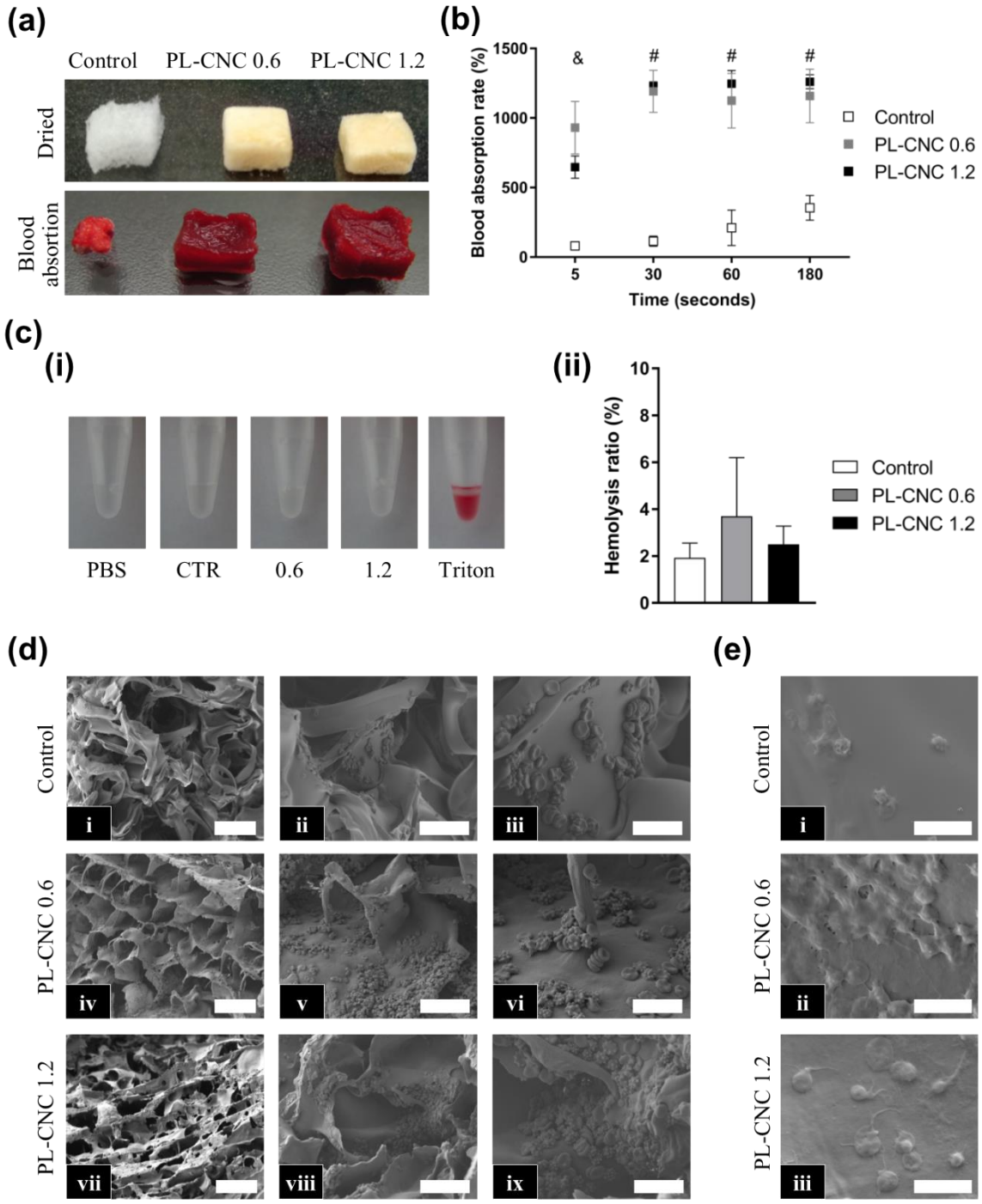

Figure 3. *In vitro* hemostatic capacity evaluation of PL-CNC cryogels compared to commercial gelatin-based hemostatic sponges (control). After 3 minutes immersion in whole blood, (a) structural shape maintenance and (b) blood absorption rate were evaluated. (c) Photographs from hemolytic activity assay (i) and hemolysis ratio (ii) of the tested formulations. SEM images of (d)

adhesion and morphology of blood cells and (e) platelets on the cryogels and commercial gelatin sponge surface. Statistical significance: $^{\&}$, $P < 0.01$, Control vs PL CNC 0.6 and $^{\#}$, $P < 0.0001$, Control vs PL CNC 0.6-1.2. Hemolysis ratio: $P = 0.6331$, PL-CNC 0.6 vs. PL-CNC 1.2; $P = 0.3984$, PL-CNC 0.6 vs. Control; and $P = 0.8949$, PL-CNC 1.2 vs Control. Scale bar: 100 µm (d-i, iv and vii), 50 µm (d-ii, v and viii), 10 µm (d-iii, vi and ix) and 5 µm (e).

In vitro cell behavior

The response of hASCs to PL-CNC cryogels and to their leachable compounds was evaluated to assess their cytocompatibility (Fig 4a and b). For this purpose, hASCs were seeded/cultured onto the cryogels without serum supplementation (i.e., FBS), Fig. 4a. Three days after seeding, live/dead assay results showed a high cell viability (> 90 %) in both PL-CNC groups, which is maintained until the end of the experiment (7 days). Moreover, hASCs presented a spindle-like morphology and were distributed within the entire cryogel network, mainly due to the structural support of PL-CNC cryogels for hASCs attachment. After 21 days in culture, hASCs exhibited high cytoskeleton elongation and extended cell spreading area, showing that the cryogels enabled an appropriate microenvironment for cells that led to well-developed cellular networks formation (Fig. S2).

hASCs were also challenged with supernatants obtained from PL-CNC 0.6, PL-CNC 1.2 and commercial gelatin formulations for 24 hours, Fig. 4b. The obtained results indicated that PL-CNC cryogel releasates collected from D0 (5 min of incubation), D0–6H and 6H–D1 significantly enhanced cell proliferation in comparison with gelatin sponge group releasates (Fig. 4b-i). At an early time interval (D0), 66 ± 13.3 % (PL-CNC 0.6) and 74.4 ± 6.6 % (PL-CNC 1.2) of PL protein content was released (Fig. 2a-ii), which likely contains relevant GFs (e.g., mitogenic

platelet-derived GF) that are able to induce cell proliferation. [67] At the subsequent time points, lower amounts of protein were released from the cryogels, resulting in minimal cell proliferation when compared with the cultures using the initial PL-CNC cryogels releasates. Moreover, cells cultured with PL-CNC cryogels supernatants at D0 exhibited a lower metabolic activity per cell in comparison with gelatin sponge (control) releasates at D0, values that are leveled for the cultures performed with the releasates of the subsequent time points, Fig. 4b-ii. Although not completely clear, we hypothesize that gelatin control releasates exhibited higher metabolic activity than PL-CNC cryogels due to their possible entrance in quiescence state, possibly induced by nutrients depravation due to the lack of FBS in the culture media.[68-70] However, further cell cycle studies would be needed to fully understand these cell behavior. Strikingly, the unique open porous structure and structural stability of PL-CNC cryogels along with bioactive cues (e.g., GFs and cytokines) presence are crucial to their excellent cytocompatibility and biofunctionality.

The effect of the soluble factors in cryogel releasates on stem cell migration and gene expression was evaluated using a scratch assay (Fig. 4c). Interactions among endogenous stem cells, tissue-resident cells and immune cells are essential factors for wound healing and regulation of the regenerative processes.[71] First, a scratch was performed in a hASCs monolayer to mimic the *in vivo* wound healing process, and subsequently the cells were treated for 48 hours with the releasates collected at D0 (Fig. 4c-I and S3). hASCs migrated faster in the presence of PL-CNC 0.6 releasates (open wound area of 0 %) when compared to hASCs in PL-CNC 1.2 (14.8 ± 29.6 %) and gelatin sponge (32.5 ± 37.6 %) releasates. We hypothesize that hASCs migrated faster in PL-CNC cryogels formulations possibly influenced by soluble PL-derived GFs that are known to promote an efficient wound closure (e.g., platelet-derived GF or stromal cell–derived factor 1α).[14, 72, 73].

The precise regulation of the wound healing response is determinant for the heathy new tissue formation.[1, 74] The process requires an adequate and controlled transition from repair to regeneration in order to avoid abnormal production of inflammatory mediators, fibrosis and ultimately promote tissue repair.[71] To evaluate the potential of our cryogels to modulate this response, the expression of α-smooth muscle actin (ACTA2), matrix metalloproteinase 9 (MMP9) and tissue inhibitor matrix metalloproteinase 1 (TIMP1) was evaluated. These makers were selected due to their importance on the degradation and turnover of the ECM that is tightly regulated by MMPs and their inhibitors (TIMPs).[75] Moreover, ACTA2 marker is associated with myofibroblast differentiation and fibrogenic conditions.[76] The gene expression results revealed that PL-CNC cryogels groups, although not statistically significant, showed a downregulation trend of scarring markers compared with gelatin group including ACTA2 and MMP9, and similar mRNA expression of TIMP1. Thus, the gene levels of the fibrosis-associated mediators ACTA2 and MMP9 tend to decrease for hASCs cells while TIMP1 is maintained, which suggests a more-regenerative and less-scarring response.

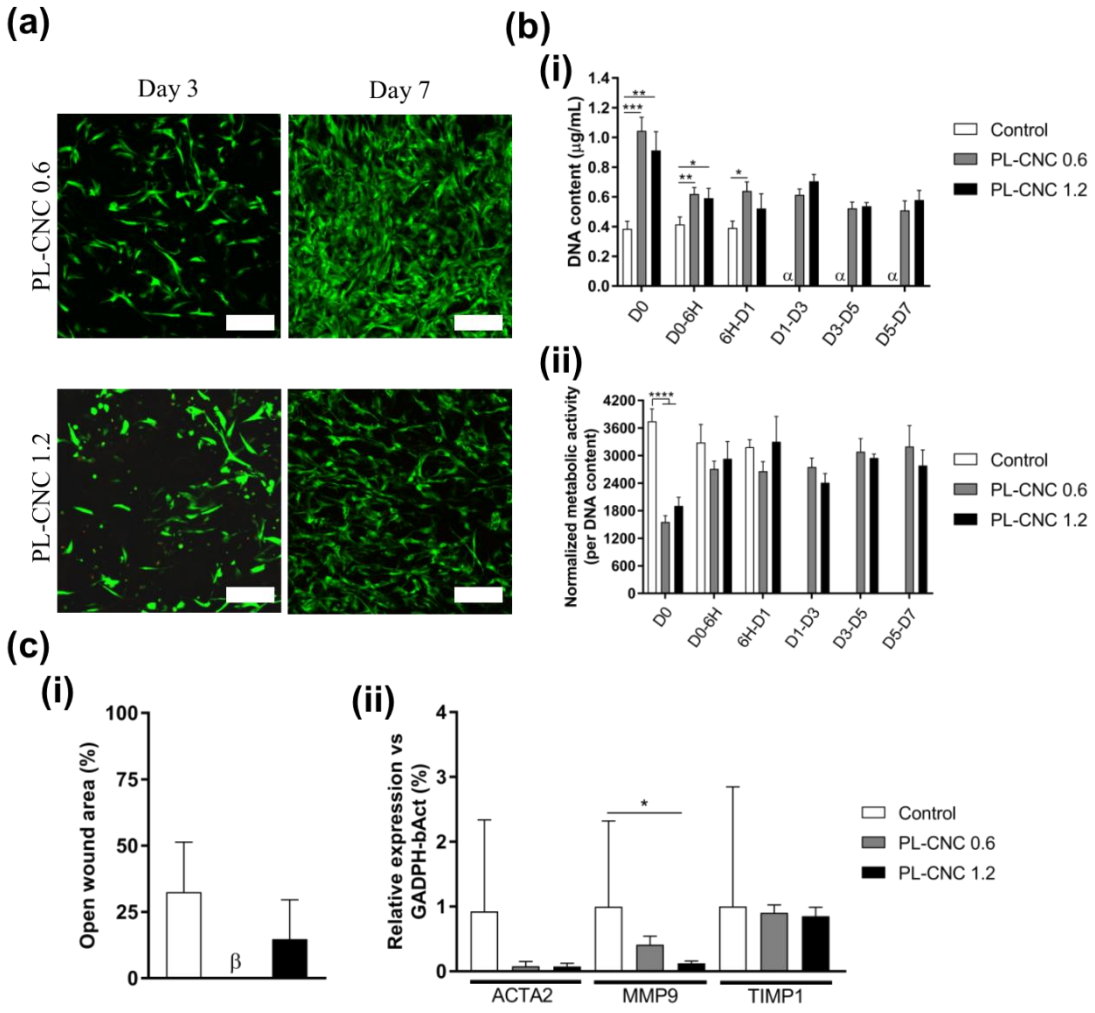

Figure 4. *In vitro* evaluation of cell supportive properties. (a) Live/Dead staining with Calcein AM and propidium iodide (green: live cells; red: dead cells) of hASCs seeded in PL-CNC cryogels after 3 and 7 days in culture. (b) DNA content (i) and metabolic activity fluorescence normalized by total DNA content (ii) of hASCs cultured with releasates of PL-CNC cryogel and gelatin sponge control (α - gelatin sponge group degraded after one day). (c) Wound healing photographs after 48 hours in culture (β - PL-CNC 0.6 formulation (n=3) showed an open wound area of 0%) (i) and gene expression of hASCs on the different formulations (ii). α-smooth muscle actin (ACTA2), matrix metalloproteinase 9 (MMP9) and tissue inhibitor matrix metalloproteinase 1 (TIMP1).

Statistical significance: *, $P < 0.1$, **, $P < 0.01$ and ***, $P < 0.001$. Scale bar: 200 µm (a) and 250 µm (b).

In vivo hemostatic performance

The hemostatic performance of PL-CNC cryogels and gelatin sponge was evaluated by bleeding time and hemorrhage volume until hemostasis was achieved (Fig 5). Liver exhibits an extremely abundant blood supply and it is susceptible to severe traumatic hemorrhaging, thus a defect in the rat lobe liver was induced, [77] and then treated with the tested formulations (Fig S3). The bleeding was controlled in 102.9 ± 31.2, 84.5 ± 58.9 and 113.6 ± 28.6 seconds after gelatin, PL-CNC 0.6 and PL-CNC 1.2 groups application, respectively (Fig. 5a-i). Until hemorrhage control, there was a blood loss of 115.8 ± 182.0 mg, 93.6 ± 38.9 mg and 65.6 ± 34.8 mg in gelatin, PL-CNC 0.6 and PL-CNC 1.2 groups, respectively (Fig. 5a-ii). Comparing the hemostasis time observed with PL-CNC cryogels to other reported hemostatic products, the improvement exceeds oxidized cellulose (Surgicel® and oxidized bacterial cellulose) and was similar to the recorded values for gelatin-based products (Kuai Kang Gelatin Sponge® and Gelita-Spon® Standard), (Fig. 5a-iii), which highlights the good hemostatic performance of PL-CNC cryogels.[29, 34]

The formulations were successfully removed from the treated injuries without rebleeding and then the adsorbed blood cells and clotting factors were analyzed (Fig. 5b). As previously observed in the *in vitro* hemocompatibility studies, a large number of RBC and platelets are rapidly recruited to the site of injury and adhered to the material surface. It is worth noticing that a fibrin network was formed in all the three formulations, which clearly enhanced blood cells absorption, platelet aggregation and effectively controlled the *in vivo* hemorrhage. The hemostatic mechanism of PL-CNC cryogels is mainly mediated by two key material features. First, human-based nanocomposite

cryogels contain an enriched milieu of platelet-derived clotting molecules that trigger platelet activation, and quickly induce blood cells adhesion, accumulation and agglomeration at the bleeding site. Moreover, PL-CNC cryogels showed a burst delivery of proteins (~70% of their initial protein content is released upon 5 minutes of incubation in an aqueous solution) containing relevant biological factors that play a significant role in antimicrobial activity and intracellular communications, thereby strengthening the blood clotting process.[14]

Remarkably, cellulose-based products have been widely applied in post-traumatic bleedings, specifically non-regenerated oxidized cellulose (e.g., Oxycel®) or regenerated oxidized cellulose (e.g., Surgicel®) gauzes.[78, 79] Here, by combining minor CNC amounts with PL-derived proteins, we are able to reproduce the strength of such materials to stop hemorrhage. These results suggest that the nanocomposite cryogels improved the hemostasis capability of such cellulose-based materials while promoting the sustained release of therapeutically-relevant proteins.

In vivo host response

When hemostatic agents are applied in the injury site, they can leave residues in the wound that can induce a severe foreign-body reaction leading to inflammation or/and thrombus.[7] PL-CNC 0.6, PL-CNC 1.2 and commercial gelatin groups were subcutaneously implanted in rats for 7 and 14 days to evaluate their *in vivo* biological response (saline solution was used as control), namely cellular infiltration and degradation behavior (Fig. 5c, d, S4 and S5). At the end of the defined timepoints, the implanted conditions and surrounding tissue were excised for histologic evaluation (Fig. 5c). After implantation for 1 week, gelatin sponges were completely absorbed, although its life-time was specified to be less than 4 weeks. Due to fast degradation, the *in vivo* response of gelatin sponge was comparable to the saline control group, thus only PL-CNC cryogels local

biological effect was evaluated (Fig. 5d). Histologic evaluation showed that both PL-CNC formulations induced inflammatory tissue reactions with different magnitudes. At day 7, the tissue reaction to the PL-CNC 0.6 formulation included a narrow band of fibrosis without fatty infiltrate (Fig. 5d-i), groups of 4-7 capillaries with supporting fibroblastic structures (Fig. 5d-ii) and moderate necrosis (Fig. 5d-iii). In contrast, the formulation with the highest CNC content induced a tissue reaction involving a moderately thick band of fibrosis without fatty infiltrate (Fig. 5d-i), minimal vascularization of its implant beds (Fig. 5d-ii) and a more severe necrosis (Fig. 5d-iii). After 14 days of implantation, both formulations showed a minimal local inflammatory response in the subcutaneous space (Fig. 5d). Interestingly, both formulations showed a low fibrosis degree, and a very low number of foreign body giant cells and neutrophils, then the overall tissue inflammatory response was significantly diminished. Our findings are in agreement with previous studies showing that CNC exhibited a mild acute inflammatory response (2 days) that was attenuated over time (30 days), indicating a good tolerance *in vivo*.[80] Although the host response was the result of the normal material-induced inflammatory tissue reaction, the observed initial inflammatory response might also be potentially caused by human PL-derived proteins. In summary, these results indicated that PL-CNC cryogels could be used as biocompatible hemostatic agents for *in vivo* application.

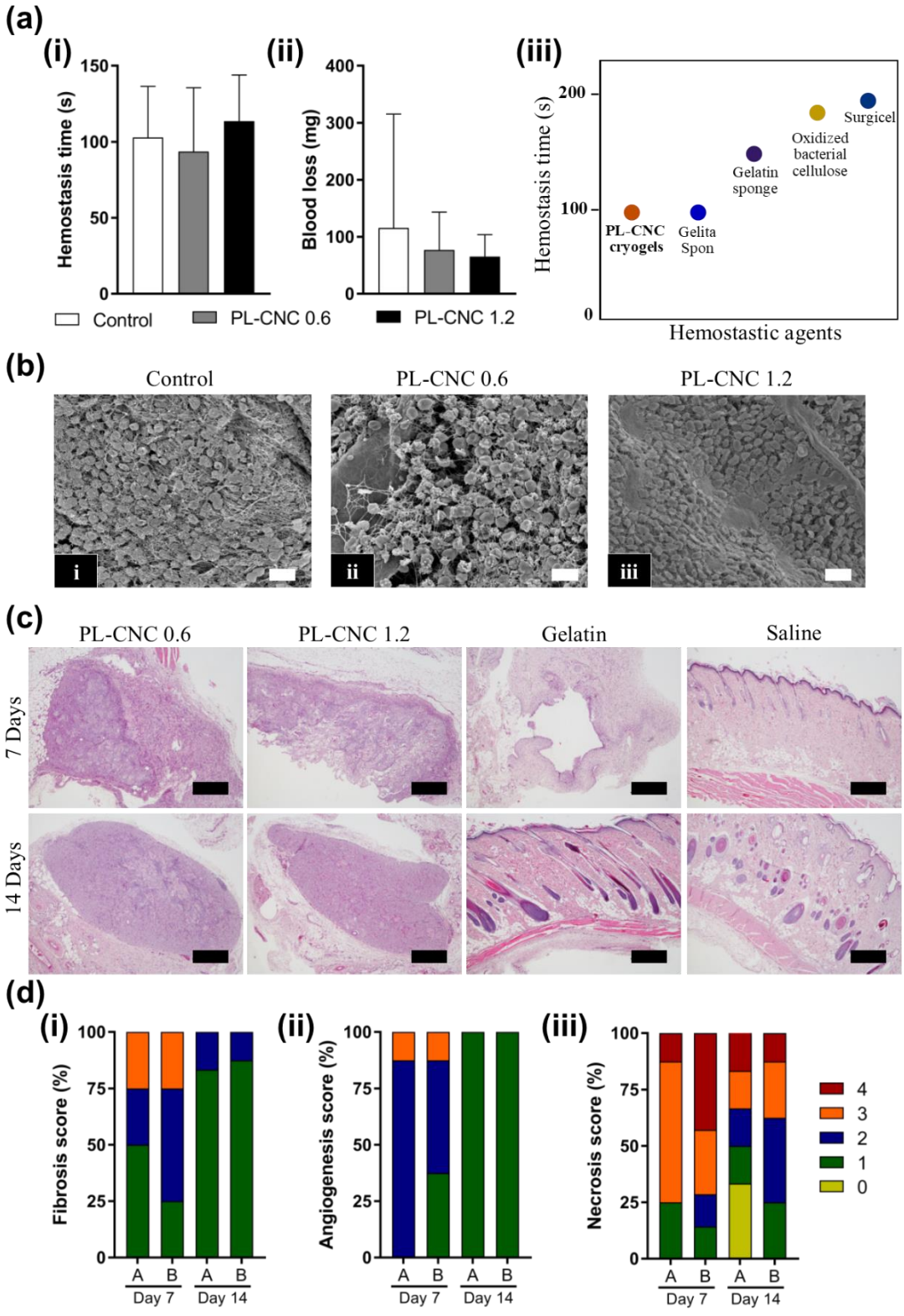
(a)
(i)
Hemostasis time (s)
150
100
50
0
Control
PL-CNC 0.6
PL-CNC 1.2
(ii)
Blood loss (mg)
400
300
200
100
0
(iii)
Hemostasis time (s)
200
100
0
PL-CNC cryogels
Gelita Spon
Gelatin sponge
Oxidized bacterial cellulose
Surgicel
Hemostastic agents
(b)
Control
PL-CNC 0.6
PL-CNC 1.2
i
ii
iii
(c)
PL-CNC 0.6
PL-CNC 1.2
Gelatin
Saline
7 Days
14 Days
(d)
(i)
Fibrosis score (%)
100
75
50
25
0
A B A B
Day 7 Day 14
(ii)
Angiogenesis score (%)
(iii)
Necrosis score (%)
4
3
2
1
0

Figure 5. *In vivo* hemostatic capacity and host response evaluation of the cryogels compared to commercial gelatin hemostatic sponges and saline solution. (a) blood loss (i), hemostatic time (ii) in the standardized liver defect model, and comparison of hemostasis time for PL-CNC cryogel and commercial products (● Surgicel® and ● oxidized bacterial cellulose[34]; and ● Kuai Kang Gelatin Sponge® [29]) (iii), (b) SEM images of surface adhesion of blood cells at the bleeding site. (c) H&E staining results of PL-CNC 0.6 and PL-CNC 1.2 cryogels, gelatin sponge and saline solution on day 7 and 14. (d) Frequency distribution of the fibrosis (i), angiogenesis (ii) and necrosis (iii) score of PL-CNC 0.6 (A) and PL-CNC 1.2 (B) groups on day 7 and 14. Scale bar: 500 μm (b) and (c).

Conclusions

The incorporation of rod-shaped CNC (0.6 to 1.2 wt.%) into the low strength PL-based network improves cryogel structural integrity, increases bulk cryogel mechanical properties and enhances the antibacterial activity against S. aureaus. In addition, PL-CNC 0.6 cryogels show a faster blood absorption rate and higher initial adhesion of platelets in comparison with PL-CNC 1.2 and gelatin formulations. Interestingly, porosity and structural integrity of PL-CNC cryogels together with the ability to deliver PL-derived bioactive molecules enables cells adhesion, increases cells migration and proliferation. The hASCs behavior upon exposure to PL-CNC cryogels releasates indicates a likely more-regenerative and less-scarring response. In a standardized liver defect model, nanocomposite cryogels showed similar hemostatic performance compared to commercial products. PL-CNC cryogels composed of small amounts of nanocellulose were not completely degraded *in vivo* due to the lack of cellulase enzymes in mammalians, but it can be incorporated in the formulations as a bioorthogonal strategy to modulate their degradation profiles. Overall,

results suggest that although the reinforcement effect of the CNC nanofillers was higher in PL-CNC 1.2, PL-CNC 0.6 cryogels showed a better hemostatic performance and might therefore be a more favorable option as hemostatic agents. In summary, the proposed PL-CNC cryogels allow the use of PL not only as a source of signaling biological factors involved in wound healing, but also as a user-friendly off-the-shelf hemostatic biomaterial with potential to promote regenerative wound healing outcomes.

ASSOCIATED CONTENT

Supporting Information. Materials and methods details. Additional physical and biological PL-CNC cryogels characterization.

AUTHOR INFORMATION

Corresponding Author

* ruimadomingues@i3bs.uminho.pt and megomes@i3bs.uminho.pt.

Author Contributions

The manuscript was written through contributions of all authors. All authors have given approval to the final version of the manuscript.

Funding Sources

This work was supported by the European Research Council; FCT/MCTES and the Norwegian Research Council.

Notes

There are no conflicts to declare.

ACKNOWLEDGMENT

The authors thank Hospital da Prelada (Porto, Portugal) for providing adipose tissue samples and Instituto Português do Sangue e Transplantação-IPST (Portugal) (Porto, Portugal) for providing platelet concentrates. The authors would like to thank Alain Morais and Isabel Pires for their support in the *in vivo* procedure and histological evaluation, respectively. The authors would like to thank the anonymous reviewers for all useful and helpful comments on our manuscript.

This work was supported by the European Research Council grant agreement No 772817; FCT/MCTES (Fundação para a Ciência e a Tecnologia/ Ministério da Ciência, Tecnologia, e Ensino Superior) and the Fundo Social Europeu através do Programa Operacional do Capital Humano (FSE/POCH) in the framework of PhD grant PD/59/2013 - PD/BD/113807/2015 (BBM) and CEECIND/01375/2017 (MGF); Norwegian Research Council for Project No. 287953.

ABBREVIATIONS

3D, three-dimensional*;* a-CNC, Aldehyde-functionalized Cellulose Nanocrystals; ACTA2, α-smooth muscle actin; AFM, Atomic Force Microscopy; *E. Coli, Escherichia coli;* ECM, Extracellular Matrix; GAPDH, glyceraldehyde-3-phosphate dehydrogenase; GF, Growth factor; hASCs, human adipose-derived stem cells; MMP, matrix metalloproteinase; μ-CT, micro-computed tomography; PBS, Phosphate-buffered saline; PL, Platelet lysate; RBC, red blood cells; RNA, Ribonucleic acid; RT, Room Temperature; *S. aureus, Staphylococcus aureus;* SEM, Scanning Electron Microscopy; TIMP, Tissue inhibitor matrix metalloproteinase.

REFERENCES

1. Gurtner, G. C.; Werner, S.; Barrandon, Y.; Longaker, M. T., Wound repair and regeneration. *Nature* **2008,** 453, (7193), 314-21.

2. Eming, S. A.; Martin, P.; Tomic-Canic, M., Wound repair and regeneration: mechanisms, signaling, and translation. *Sci. Transl. Med.* **2014,** 6, (265), 265sr6.

3. Tomaiuolo, M.; Brass, L. F.; Stalker, T. J., Regulation of Platelet Activation and Coagulation and Its Role in Vascular Injury and Arterial Thrombosis. *Interv. Cardiol. Clin.* **2017,** 6, (1), 1-12.

4. Weisel, J. W.; Litvinov, R. I., Mechanisms of fibrin polymerization and clinical implications. *Blood* **2013,** 121, (10), 1712-1719.

5. Sauaia, A.; Moore, F. A.; Moore, E. E.; Moser, K. S.; Brennan, R.; Read, R. A.; Pons, P. T., Epidemiology of Trauma Deaths: A Reassessment. *J. Trauma Acute Care Surg.* **1995,** 38, (2), 185-193.

6. Kauvar, D. S.; Lefering, R.; Wade, C. E., Impact of hemorrhage on trauma outcome: an overview of epidemiology, clinical presentations, and therapeutic considerations. *J. Trauma Acute Care Surg.* **2006,** 60, (6), S3-S11.

7. Khoshmohabat, H.; Paydar, S.; Kazemi, H. M.; Dalfardi, B., Overview of Agents Used for Emergency Hemostasis. *Trauma Mon.* **2016,** 21, (1), e26023-e26023.

8. Morrison, C. A., The prehospital treatment of the bleeding patient. Dare to dream. *J. Surg. Res.* **2013,** 180, (2), 246-247.

9. Devlin, J. J.; Kircher, S.; Kozen, B. G.; Littlejohn, L. F.; Johnson, A. S., Comparison of ChitoFlex®, CELOX™, and QuikClot® in Control of Hemorrhage. *J. Emerg. Med.* **2011,** 41, (3), 237-245.

10. Rhee, P.; Brown, C.; Martin, M.; Salim, A.; Plurad, D.; Green, D.; Chambers, L.; Demetriades, D.; Velmahos, G.; Alam, H., QuikClot Use in Trauma for Hemorrhage Control: Case Series of 103 Documented Uses. *J. Trauma Acute Care Surg.* **2008,** 64, (4), 1093-1099.

11. Reiss, R. F.; Oz, M. C., Autologous fibrin glue: Production and clinical use. *Transfus. Med. Rev.* **1996,** 10, (2), 85-92.

12. Pavlovic, V.; Ciric, M.; Jovanovic, V.; Stojanovic, P., Platelet Rich Plasma: a short overview of certain bioactive components. *Open Med. J.* **2016,** 11, (1), 242-247.

13. Boswell, S. G.; Cole, B. J.; Sundman, E. A.; Karas, V.; Fortier, L. A., Platelet-Rich Plasma: A Milieu of Bioactive Factors. *Arthroscopy* **2012,** 28, (3), 429-439.

14. Mendes, B. B.; Gómez-Florit, M.; Babo, P. S.; Domingues, R. M.; Reis, R. L.; Gomes, M. E., Blood derivatives awaken in regenerative medicine strategies to modulate wound healing. *Adv. Drug Deliv. Rev.* **2018,** 129, 376-393.

15. Flaumenhaft, R., Chapter 18 - Platelet Secretion. In *Platelets (Third Edition)*, Michelson, A. D., Ed. Academic Press: 2013; pp 343-366.

16. Jung, H.; Kang, Y. Y.; Mok, H., Platelet-derived nanovesicles for hemostasis without release of pro-inflammatory cytokines. *Biomater. Sci.* **2019,** 7, (3), 856-859.

17. Hawksworth, J. S.; Elster, E. A.; Fryer, D.; Sheppard, F.; Morthole, V.; Krishnamurthy, G.; Tomori, T.; Brown, T. S.; Tadaki, D. K., Evaluation of lyophilized platelets as an infusible

hemostatic agent in experimental non-compressible hemorrhage in swine. *J. Thromb. Haemost.* **2009,** 7, (10), 1663-1671.

18. Brown, A. C.; Stabenfeldt, S. E.; Ahn, B.; Hannan, R. T.; Dhada, K. S.; Herman, E. S.; Stefanelli, V.; Guzzetta, N.; Alexeev, A.; Lam, W. A.; Lyon, L. A.; Barker, T. H., Ultrasoft microgels displaying emergent platelet-like behaviours. *Nat. Mater.* **2014,** 13, (12), 1108-1114.

19. Behrens, A. M.; Sikorski, M. J.; Kofinas, P., Hemostatic strategies for traumatic and surgical bleeding. *J. Biomed. Mater. Res.* **2014,** 102, (11), 4182-4194.

20. Sekhon, U. D. S.; Sen Gupta, A., Platelets and Platelet-Inspired Biomaterials Technologies in Wound Healing Applications. *ACS Biomater. Sci. Eng.* **2018,** 4, (4), 1176-1192.

21. Rossi, S.; Faccendini, A.; Bonferoni, M. C.; Ferrari, F.; Sandri, G.; Del Fante, C.; Perotti, C.; Caramella, C. M., "Sponge-like" dressings based on biopolymers for the delivery of platelet lysate to skin chronic wounds. *Int. J. Pharm.* **2013,** 440, (2), 207-215.

22. Nardini, M.; Perteghella, S.; Mastracci, L.; Grillo, F.; Marrubini, G.; Bari, E.; Formica, M.; Gentili, C.; Cancedda, R.; Torre, M. L.; Mastrogiacomo, M., Growth Factors Delivery System for Skin Regeneration: An Advanced Wound Dressing. *Pharmaceutics* **2020,** 12, (2), 120.

23. Qu, J.; Zhao, X.; Liang, Y.; Zhang, T.; Ma, P. X.; Guo, B., Antibacterial adhesive injectable hydrogels with rapid self-healing, extensibility and compressibility as wound dressing for joints skin wound healing. *Biomaterials* **2018,** 183, 185-199.

24. He, J.; Shi, M.; Liang, Y.; Guo, B., Conductive adhesive self-healing nanocomposite hydrogel wound dressing for photothermal therapy of infected full-thickness skin wounds. *Chem. Eng. J.* **2020,** 394, 124888.

25. Zhao, X.; Guo, B.; Wu, H.; Liang, Y.; Ma, P. X., Injectable antibacterial conductive nanocomposite cryogels with rapid shape recovery for noncompressible hemorrhage and wound healing. *Nat. Commun.* **2018,** 9, (1), 2784.

26. Memic, A.; Colombani, T.; Eggermont, L. J.; Rezaeeyazdi, M.; Steingold, J.; Rogers, Z. J.; Navare, K. J.; Mohammed, H. S.; Bencherif, S. A., Latest Advances in Cryogel Technology for Biomedical Applications. *Adv. Ther.* **2019,** 2, (4), 1800114.

27. Koshy, S. T.; Ferrante, T. C.; Lewin, S. A.; Mooney, D. J., Injectable, porous, and cell-responsive gelatin cryogels. *Biomaterials* **2014,** 35, (8), 2477-2487.

28. Bencherif, S. A.; Warren Sands, R.; Ali, O. A.; Li, W. A.; Lewin, S. A.; Braschler, T. M.; Shih, T.-Y.; Verbeke, C. S.; Bhatta, D.; Dranoff, G.; Mooney, D. J., Injectable cryogel-based whole-cell cancer vaccines. *Nature Commun.* **2015,** 6, (1), 7556.

29. Yang, X.; Liu, W.; Shi, Y.; Xi, G.; Wang, M.; Liang, B.; Feng, Y.; Ren, X.; Shi, C., Peptide-immobilized starch/PEG sponge with rapid shape recovery and dual-function for both uncontrolled and noncompressible hemorrhage. *Acta Biomater.* **2019,** 99, 220-235.

30. Domingues, R. M. A.; Gomes, M. E.; Reis, R. L., The Potential of Cellulose Nanocrystals in Tissue Engineering Strategies. *Biomacromolecules* **2014,** 15, (7), 2327-2346.

31. Foster, E. J.; Moon, R. J.; Agarwal, U. P.; Bortner, M. J.; Bras, J.; Camarero-Espinosa, S.; Chan, K. J.; Clift, M. J. D.; Cranston, E. D.; Eichhorn, S. J.; Fox, D. M.; Hamad, W. Y.; Heux, L.; Jean, B.; Korey, M.; Nieh, W.; Ong, K. J.; Reid, M. S.; Renneckar, S.; Roberts, R.; Shatkin, J. A.; Simonsen, J.; Stinson-Bagby, K.; Wanasekara, N.; Youngblood, J., Current characterization methods for cellulose nanomaterials. *Chem. Soc. Rev.* **2018,** 47, (8), 2609-2679.

32. Motealleh, A.; Kehr, N. S., Nanocomposite Hydrogels and Their Applications in Tissue Engineering. *Adv. Healthc. Mater.* **2017,** 6, (1), 1600938.

33. Cheng, F.; Liu, C.; Wei, X.; Yan, T.; Li, H.; He, J.; Huang, Y., Preparation and Characterization of 2,2,6,6-Tetramethylpiperidine-1-oxyl (TEMPO)-Oxidized Cellulose Nanocrystal/Alginate Biodegradable Composite Dressing for Hemostasis Applications. *ACS Sustain. Chem. Eng.* **2017,** 5, (5), 3819-3828.

34. Yuan, H.; Chen, L.; Hong, F. F., A Biodegradable Antibacterial Nanocomposite Based on Oxidized Bacterial Nanocellulose for Rapid Hemostasis and Wound Healing. *ACS Appl. Mater. Inter.* **2020,** 12, (3), 3382-3392.

35. Mendes, B. B.; Gómez-Florit, M.; Pires, R. A.; Domingues, R. M. A.; Reis, R. L.; Gomes, M. E., Human-based fibrillar nanocomposite hydrogels as bioinstructive matrices to tune stem cell behavior. *Nanoscale* **2018,** 10, (36), 17388-17401.

36. Bondeson, D.; Mathew, A.; Oksman, K., Optimization of the isolation of nanocrystals from microcrystalline celluloseby acid hydrolysis. *Cellulose* **2006,** 13, (2), 171.

37. Domingues, R. M. A.; Silva, M.; Gershovich, P.; Betta, S.; Babo, P.; Caridade, S. G.; Mano, J. F.; Motta, A.; Reis, R. L.; Gomes, M. E., Development of Injectable Hyaluronic Acid/Cellulose Nanocrystals Bionanocomposite Hydrogels for Tissue Engineering Applications. *Bioconjug. Chem.* **2015,** 26, (8), 1571-1581.

38. Zhao, X.; Wu, H.; Guo, B.; Dong, R.; Qiu, Y.; Ma, P. X., Antibacterial anti-oxidant electroactive injectable hydrogel as self-healing wound dressing with hemostasis and adhesiveness for cutaneous wound healing. *Biomaterials* **2017,** 122, 34-47.

39. Chen, Z.; Han, L.; Liu, C.; Du, Y.; Hu, X.; Du, G.; Shan, C.; Yang, K.; Wang, C.; Li, M.; Li, F.; Tian, F., A rapid hemostatic sponge based on large, mesoporous silica nanoparticles and N-alkylated chitosan. *Nanoscale* **2018,** 10, (43), 20234-20245.

40. Carvalho, P. P.; Wu, X.; Yu, G.; Dias, I. R.; Gomes, M. E.; Reis, R. L.; Gimble, J. M., The effect of storage time on adipose-derived stem cell recovery from human lipoaspirates. *Cells Tissues Organs* **2011,** 194, (6), 494-500.

41. Liang, C.-C.; Park, A. Y.; Guan, J.-L., In vitro scratch assay: a convenient and inexpensive method for analysis of cell migration in vitro. *Nat. Protoc.* **2007,** 2, (2), 329-333.

42. Taylor, S. C.; Nadeau, K.; Abbasi, M.; Lachance, C.; Nguyen, M.; Fenrich, J., The Ultimate qPCR Experiment: Producing Publication Quality, Reproducible Data the First Time. *Trends Biotechnol.* **2019,** 37, (7), 761-774.

43. Viau, S.; Lagrange, A.; Chabrand, L.; Lorant, J.; Charrier, M.; Rouger, K.; Alvarez, I.; Eap, S.; Delorme, B., A highly standardized and characterized human platelet lysate for efficient and reproducible expansion of human bone marrow mesenchymal stromal cells. *Cytotherapy* **2019,** 21, (7), 738-754.

44. Wu, J.; Zhao, Q.; Sun, J.; Zhou, Q., Preparation of poly(ethylene glycol) aligned porous cryogels using a unidirectional freezing technique. *Soft Matter* **2012,** 8, (13), 3620-3626.

45. Lozinsky, V. I.; Galaev, I. Y.; Plieva, F. M.; Savina, I. N.; Jungvid, H.; Mattiasson, B., Polymeric cryogels as promising materials of biotechnological interest. *Trends Biotechnol.* **2003,** 21, (10), 445-451.

46. Chau, M.; De France, K. J.; Kopera, B.; Machado, V. R.; Rosenfeldt, S.; Reyes, L.; Chan, K. J. W.; Förster, S.; Cranston, E. D.; Hoare, T.; Kumacheva, E., Composite Hydrogels with Tunable Anisotropic Morphologies and Mechanical Properties. *Chem. Mater.* **2016,** 28, (10), 3406-3415.

47. Dash, R.; Foston, M.; Ragauskas, A. J., Improving the mechanical and thermal properties of gelatin hydrogels cross-linked by cellulose nanowhiskers. *Carbohydr. Polym.* **2013,** 91, (2), 638-645.

48. Henderson, T. M. A.; Ladewig, K.; Haylock, D. N.; McLean, K. M.; O'Connor, A. J., Cryogels for biomedical applications. *J. Mater. Chem. B* **2013,** 1, (21), 2682-2695.

49. Liu, Y.; Xu, K.; Chang, Q.; Darabi, M. A.; Lin, B.; Zhong, W.; Xing, M., Highly Flexible and Resilient Elastin Hybrid Cryogels with Shape Memory, Injectability, Conductivity, and Magnetic Responsive Properties. *Adv. Mater.* **2016,** 28, (35), 7758-7767.

50. Mueller, G. R.; Pineda, T. J.; Xie, H. X.; Teach, J. S.; Barofsky, A. D.; Schmid, J. R.; Gregory, K. W., A novel sponge-based wound stasis dressing to treat lethal noncompressible hemorrhage. *J. Trauma Acute Care Surg.* **2012,** 73, (2 Suppl 1), S134-9.

51. Sorrentino, S.; Studt, J.-D.; Medalia, O.; Tanuj Sapra, K., Roll, adhere, spread and contract: Structural mechanics of platelet function. *Eur. J. Cell Biol.* **2015,** 94, (3), 129-138.

52. Neveleff, D. J., Optimizing Hemostatic Practices: Matching the Appropriate Hemostat to the Clinical Situation. *AORN J.* **2012,** 96, (5), S1-S17.

53. Babo, P. S.; Santo, V. E.; Gomes, M. E.; Reis, R. L., Development of an Injectable Calcium Phosphate/Hyaluronic Acid Microparticles System for Platelet Lysate Sustained Delivery Aiming Bone Regeneration. *Macromol. Biosci.* **2016,** 16, (11), 1662-1677.

54. Arifin, D. Y.; Lee, L. Y.; Wang, C.-H., Mathematical modeling and simulation of drug release from microspheres: Implications to drug delivery systems. *Adv. Drug Deliv. Rev.s* **2006,** 58, (12), 1274-1325.

55. Silva, C. R.; Babo, P. S.; Gulino, M.; Costa, L.; Oliveira, J. M.; Silva-Correia, J.; Domingues, R. M. A.; Reis, R. L.; Gomes, M. E., Injectable and tunable hyaluronic acid hydrogels releasing chemotactic and angiogenic growth factors for endodontic regeneration. *Acta Biomater.* **2018,** 77, 155-171.

56. Fortunato, T. M.; Beltrami, C.; Emanueli, C.; De Bank, P. A.; Pula, G., Platelet lysate gel and endothelial progenitors stimulate microvascular network formation in vitro: tissue engineering implications. *Sci. Rep.* **2016,** 6, (1), 25326.

57. Yeaman, M. R., Platelets in defense against bacterial pathogens. *Cell Mol. Life Sci.* **2010,** 67, (4), 525-544.

58. Tang, Y.-Q.; Yeaman, M. R.; Selsted, M. E., Antimicrobial peptides from human platelets. *Infect. Immun.* **2002,** 70, (12), 6524-6533.

59. Chung, P. Y.; Khanum, R., Antimicrobial peptides as potential anti-biofilm agents against multidrug-resistant bacteria. *J. Microbiol. Immunol. Infect.* **2017,** 50, (4), 405-410.

60. Costa-Almeida, R.; Franco, A. R.; Pesqueira, T.; Oliveira, M. B.; Babo, P. S.; Leonor, I. B.; Mano, J. F.; Reis, R. L.; Gomes, M. E., The effects of platelet lysate patches on the activity of tendon-derived cells. *Acta Biomater.* **2018,** 68, 29-40.

61. Mendes, B. B.; Gómez-Florit, M.; Osório, H.; Vilaça, A.; Domingues, R. M. A.; Reis, R. L.; Gomes, M. E., Cellulose nanocrystals of variable sulfation degrees can sequester specific platelet lysate-derived biomolecules to modulate stem cell response. *Chem. Commun.* **2020,** 56, (50), 6882-6885.

62. Teixeira, S. P. B.; Domingues, R. M. A.; Shevchuk, M.; Gomes, M. E.; Peppas, N. A.; Reis, R. L., Biomaterials for Sequestration of Growth Factors and Modulation of Cell Behavior. *Adv. Funct. Mater.* **2020,** 1909011.

63. Schaer, D. J.; Buehler, P. W.; Alayash, A. I.; Belcher, J. D.; Vercellotti, G. M., Hemolysis and free hemoglobin revisited: exploring hemoglobin and hemin scavengers as a novel class of therapeutic proteins. *Blood* **2013,** 121, (8), 1276-1284.

64. Wagner, C.; Steffen, P.; Svetina, S., Aggregation of red blood cells: From rouleaux to clot formation. *C. R. Phys.* **2013,** 14, (6), 459-469.

65. Bessis, M. In *Red Cell Shapes. An Illustrated Classification and its Rationale*, Red Cell Shape, Berlin, Heidelberg, 1973//, 1973; Bessis, M.; Weed, R. I.; Leblond, P. F., Eds. Springer Berlin Heidelberg: Berlin, Heidelberg, 1973; pp 1-25.

66. Yun, S.-H.; Sim, E.-H.; Goh, R.-Y.; Park, J.-I.; Han, J.-Y., Platelet Activation: The Mechanisms and Potential Biomarkers. *Biomed. Res. Int.* **2016,** 2016, 9060143-9060143.

67. Lai, F.; Kakudo, N.; Morimoto, N.; Taketani, S.; Hara, T.; Ogawa, T.; Kusumoto, K., Platelet-rich plasma enhances the proliferation of human adipose stem cells through multiple signaling pathways. *Stem Cell Res. Ther.* **2018,** 9, (1), 107.

68. Coller, H. A., The paradox of metabolism in quiescent stem cells. *FEBS Lett.* **2019,** 593, (20), 2817-2839.

69. Shyh-Chang, N.; Daley, G. Q.; Cantley, L. C., Stem cell metabolism in tissue development and aging. *Development* **2013,** 140, (12), 2535.

70. Valcourt, J. R.; Lemons, J. M. S.; Haley, E. M.; Kojima, M.; Demuren, O. O.; Coller, H. A., Staying alive: metabolic adaptations to quiescence. *Cell Cycle* **2012,** 11, (9), 1680-1696.

71. Xia, H.; Li, X.; Gao, W.; Fu, X.; Fang, R. H.; Zhang, L.; Zhang, K., Tissue repair and regeneration with endogenous stem cells. *Nat. Rev. Mater.* **2018,** 3, (7), 174-193.

72. Ranzato, E.; Mazzucco, L.; Patrone, M.; Burlando, B., Platelet lysate promotes in vitro wound scratch closure of human dermal fibroblasts: different roles of cell calcium, P38, ERK and PI3K/AKT. *J. Cell. Mol. Med.* **2009,** 13, (8b), 2030-2038.

73. Massberg, S.; Konrad, I.; Schürzinger, K.; Lorenz, M.; Schneider, S.; Zohlnhoefer, D.; Hoppe, K.; Schiemann, M.; Kennerknecht, E.; Sauer, S.; Schulz, C.; Kerstan, S.; Rudelius, M.; Seidl, S.; Sorge, F.; Langer, H.; Peluso, M.; Goyal, P.; Vestweber, D.; Emambokus, N. R.; Busch, D. H.; Frampton, J.; Gawaz, M., Platelets secrete stromal cell-derived factor 1alpha and recruit bone marrow-derived progenitor cells to arterial thrombi in vivo. *J. Exp. Med.* **2006,** 203, (5), 1221-1233.

74. Forbes, S. J.; Rosenthal, N., Preparing the ground for tissue regeneration: from mechanism to therapy. *Nat. Med.* **2014,** 20, (8), 857-69.

75. O'Sullivan, S.; Gilmer, J. F.; Medina, C., Matrix metalloproteinases in inflammatory bowel disease: an update. *Mediators Inflamm.* **2015,** 2015, 964131-964131.

76. Hinz, B.; Phan, S. H.; Thannickal, V. J.; Galli, A.; Bochaton-Piallat, M.-L.; Gabbiani, G., The myofibroblast: one function, multiple origins. *Am. J. Pathol.* **2007,** 170, (6), 1807-1816.

77. Ahmed, N.; Vernick, J. J., Management of liver trauma in adults. *J. Emerg. Trauma Shock* **2011,** 4, (1), 114-119.

78. Lewis, K. M.; Spazierer, D.; Urban, M. D.; Lin, L.; Redl, H.; Goppelt, A., Comparison of regenerated and non-regenerated oxidized cellulose hemostatic agents. *Eur. Surg.* **2013,** 45, (4), 213-220.

79. Yang, X.; Liu, W.; Li, N.; Wang, M.; Liang, B.; Ullah, I.; Luis Neve, A.; Feng, Y.; Chen, H.; Shi, C., Design and development of polysaccharide hemostatic materials and their hemostatic mechanism. *Biomater. Sci.* **2017,** 5, (12), 2357-2368.

80. De France, K. J.; Badv, M.; Dorogin, J.; Siebers, E.; Panchal, V.; Babi, M.; Moran-Mirabal, J.; Lawlor, M.; Cranston, E. D.; Hoare, T., Tissue Response and Biodistribution of Injectable Cellulose Nanocrystal Composite Hydrogels. *ACS Biomater. Sci. Eng.* **2019**, 5, (5), 2235-2246.

Table of Contents Graphic